CFD Modeling and Rheological Calibration of Lubricating Grease

Lorenzo Maccioni[1, a)], Michele Benetti[1], Michael Plogmann[2], Kay Juckelandt[2], Franco Concli[1]

[1]*Free University of Bozen-Bolzano, Faculty of Engineering, via Bruno Buozzi 1, 39100, Bolzano, Italy.*
[2]*Schaeffler Technologies AG & Co. KG, Industriestrasse 1–3, 91074 Herzogenaurach, Germany*

[a)] Corresponding author: lorenzo.maccioni@unibz.it

Abstract. This work presents a methodology to calibrate and verify the Herschel–Bulkley rheological model for lubricating greases in the context of Computational Fluid Dynamics (CFD). The approach combines Cone-on-Plate and Plate-on-Plate rheometry with numerical simulations to derive temperature-dependent model parameters and assess their predictive fidelity. Experimental measurements were conducted on an NLGI 1 grease for bearings application at 25 °C and 80 °C, covering a broad range of shear rates. Multiple regression strategies were tested, showing that the choice of error metric significantly affects model predictions, with logarithmic error minimization providing the most robust results across conditions. CFD validation was first carried out on the Cone-on-Plate configuration, yielding excellent agreement with both analytical Herschel–Bulkley predictions and experiments. The Plate-on-Plate setup introduced additional complexity due to shear rate gradients and higher edge effects. Comparisons demonstrated good agreement at elevated temperatures and small gaps, while larger discrepancies emerged at ambient temperature and wider gaps, with CFD generally overestimating torque. The findings highlight both the strengths and current limitations of the proposed approach for modeling grease-lubricated systems, and underscore the importance of temperature calibration protocols to enhance predictive accuracy in CFD analyses of grease-lubricated components such as rolling element bearings.

INTRODUCTION

Computational Fluid Dynamics (CFD) has become a fundamental design tool for analyzing lubricated mechanical systems such as bearings and gear trains [1]. Integrating CFD into the design process can significantly reduce the cost and duration of experimental campaigns [2], while enabling quantitative predictions of lubricant fluxes within components [3, 4], load-independent power losses induced by viscous and inertial effects [5, 6], and the static and dynamic forces exerted by the fluids on interacting parts [7].

Although more than 80% of rolling element bearings are grease-lubricated [8, 9], most CFD studies still focus on oil-lubricated bearings [1]. Where grease is considered, it is frequently idealized as a static reservoir that bleeds base oil, and the ensuing oil flow is modeled with Newtonian rheology. Representative examples include the works of Zhang et al. [10-12] and Fischer et al. [13], which simulate the ball–raceway contact to study oil bleeding, replenishment, and starvation, but treat the grease as an oil source and adopt Newtonian models for the fluid phase. Similarly, Wang [14] identified active grease reservoirs in angular-contact bearings by prescribing fixed grease pockets and simulating oil bleeding with Newtonian assumptions. Such approaches sidestep the non-Newtonian character of grease, whose response depends on temperature, pre-shear history, and aging [15-18]; dependencies that are crucial under in-service conditions.

Grease characterization is often performed with methods that do not reflect operating environments. The solid-like resistance to flow is traditionally assessed via cone penetration tests [19, 20], which yield an NLGI consistency number but not a constitutive model. Yield stress can be estimated with rheometers using computerized evaluation (e.g., CEY by Gow [21]) or stress-crossover techniques (e.g., Couronné et al. [22]), yet these measurements are typically conducted at room temperature and rarely account for in-service temperatures, shear histories, or aging. Several constitutive equations have been proposed to describe grease over a range of shear rates: including Power-

Law [23], Rhee–Eyring [24], Bingham [25, 26], Papanastasiou [27], and Herschel–Bulkley [28] models. Among the above-mentioned Herschel–Bulkley is particularly suitable for mechanical-component simulations because it combines a yield-stress threshold with a shear-thinning power-law term [29].

A growing body of research attempts to incorporate non-Newtonian behavior into CFD for bearings, yet key gaps remain. Raj et al. [30] modeled a roller-bearing channel using the Herschel–Bulkley law, calibrated via Plate-on-Plate rheometer. However, the parameters were measured at a single temperature and implicitly assumed to be temperature independent. Moreover, between 2016 and 2020, Noda et al. [31, 32] treated grease as a two-phase fluid governed by the Papanastasiou regularization of a viscoplastic law and complemented simulations with X-ray CT experiments. Nevertheless, the authors did not discuss potential discrepancies arising from differences between calibration and test temperatures. In another study, Wang et al. analyzed coupled thermo-fluid behavior in high-speed angular-contact ball bearings lubricated with grease, modeling the lubricant with the Herschel–Bulkley law [33]. However, the Herschel–Bulkley parameters were taken directly from the literature, with no dedicated experimental calibration and no treatment of temperature dependence. A similar approach was adopted by Fu et al., who performed CFD of grease lubrication in double-row spherical roller bearings using data from the literature [34]. These practices underscore the importance of laboratory protocols that enable in-house calibration of grease rheology and for broader datasets reporting grease properties across multiple temperatures.

The objective of this paper is to provide a practical methodology to calibrate the Herschel–Bulkley rheological model for bearing greases and to verify its consistency and reliability within CFD analyses. We explicitly examine experimental and numerical considerations — such as temperature dependence, pre-shear, and measurement protocols — and delineate the limitations of common practices. By bridging rheometry and simulation, the proposed framework aims to enable physically grounded, reproducible grease models that improve the predictive fidelity of CFD for grease-lubricated bearings.

RESEARCH METHODOLOGY

This chapter summarizes the methodological framework adopted in the study, which provides the basis for the partial results presented in the subsequent sections. The overall aim of the research is to calibrate the Herschel–Bulkley model for use in CFD, to accurately predict the rheological behavior of lubricating grease under controlled conditions.

The Herschel–Bulkley constitutive equation is expressed as:

$$\tau(\dot{\gamma}) = \tau_0 + K \cdot \dot{\gamma}^n \tag{1}$$

where:

- $\tau(\dot{\gamma})$ = shear stress [Pa]
- $\dot{\gamma}$ = shear rate [s^{-1}]
- τ_0 = yield stress [Pa]
- K = consistency index [$Pa \cdot s^n$]
- n = flow index [-]

From this relation, one possible definition of viscosity is given by:

$$\mu(\dot{\gamma}) = min\left\{\frac{\tau_0}{\dot{\gamma}} + K \cdot \dot{\gamma}^{n-1}, \mu_0\right\} \tag{2}$$

where μ_0 represents the zero-shear viscosity of the grease. This modification prevents the model from producing singularities and numerical instabilities at very low shear rates.

The experimental calibration was performed at two reference temperatures:

- 25 [°C], representing ambient conditions, and
- 80 [°C], representative of a possible operating environment.

A Cone-on-Plate rheometer was selected for these measurements, as this configuration allows testing a finite sample volume while maintaining a uniform shear rate throughout the material. Torque (T) and angular velocity (ω) data collected during the experiments were converted into shear stress $\tau(\dot{\gamma})$ and shear rate $\dot{\gamma}$ values using the instrument-specific CSS and CSR calibration coefficients, coefficients released by the rheometer producer.

Once the experimental τ-$\dot{\gamma}$ datasets were obtained, regression techniques were applied to fit the Herschel–Bulkley parameters, i.e. (τ_0, K, n). Different regression strategies were tested to minimize various error functions, including:

- Mean Squared Error (MSE),
- Absolute Error,
- Percentage Error,
- Logarithmic Error.

The comparison of these approaches demonstrated that the choice of error metric influences the final parameter set, yielding slightly different model predictions.

After calibration, the constitutive model was implemented in a CFD framework. The first step of validation consisted of reproducing the Cone-on-Plate rheometer setup numerically. The model was considered consistent when the CFD results showed:

- an approximately uniform shear rate across the test volume, and
- a torque–angular velocity relationship in agreement with the analytical Herschel–Bulkley formulation.

A second validation stage was conducted using a Plate-on-Plate rheometer, which introduces shear rate gradients that increase radially. An additional experimental campaign was carried out with this geometry, testing the same grease at both reference temperatures and at varying plate gaps and rotation speeds. The Plate-on-Plate configuration was also modeled in CFD using the previously calibrated fluid properties.

Comparisons between the experimentally measured and CFD-predicted torque–angular velocity curves allowed for assessment of the model accuracy, identification of discrepancies, and formulation of hypotheses regarding their possible origins.

EXPERIMENTAL CAMPAIGN AND DATA ELABORATION

As outlined in the previous section, the experimental campaign was conducted using the same NLGI 1 grease, tested in two different rheometer configurations: Cone-on-Plate and Plate-on-Plate. Measurements were performed under different temperatures and angular velocities. Specifically, tests were carried out with $\omega = 1.76 \cdot 10^{-3} \div 1.76 \cdot 10^{1}\ [rad/s]$ in the Cone-on-Plate setup, and $\omega = 6.00 \cdot 10^{-1} \div 1.20 \cdot 10^{2}\ [rad/s]$ in the Plate-on-Plate setup. These conditions correspond to shear rates spanning from $\dot{\gamma} = 1 \cdot 10^{-1} \div 1 \cdot 10^{3}\ [s^{-1}]$. All measurements were carried out in accordance with DIN 51810-1. For the Cone-on-Plate configuration, 41 data points were collected at each velocity following a geometric progression with a ratio of approximately 1.25, whereas in the Plate-on-Plate configuration, 31 measurements were obtained using an arithmetic progression with an increment of about 2 between successive velocities.

The tests were conducted on grease samples that had not been subjected to pre-shearing. Each experiment consisted of three phases: an acceleration phase up to the maximum velocity, a steady-state phase during which the maximum velocity was maintained for 10 minutes, and eventually a deceleration phase. For subsequent data processing, only the acceleration-phase data were considered, in order to analyze the grease without pre-shearing effects. It should be noted, however, that deceleration data differed by up to 15% compared to acceleration, with the latter generally showing a higher resisting torque.

In the Cone-on-Plate tests, measurements were performed at 25 [°C] and 80 [°C], as well as at intermediate temperatures of 30 [°C] and 70 [°C], in order to assess the influence of small variations in thermal conditions (i.e., +5 [°C] near ambient and −10 [°C] near operating conditions). These tests revealed that even relatively modest temperature shifts could lead to torque–angular velocity deviations exceeding 20%, particularly at high angular velocities (Fig. 1).

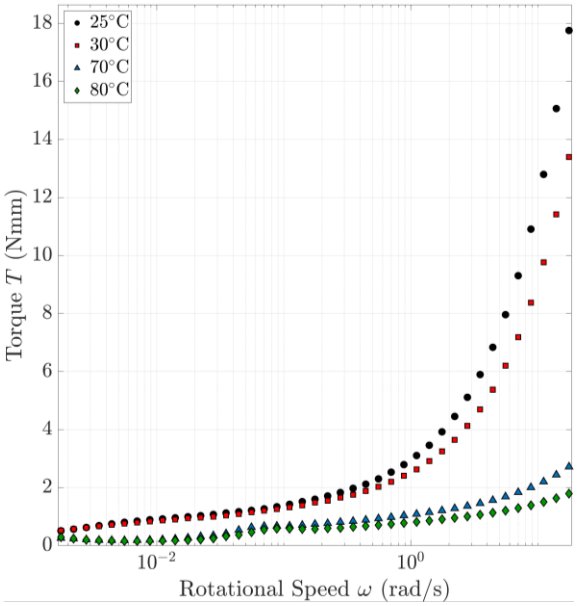

FIGURE 1. Rotational speed vs Torque for different temperatures in Cone-on-Plate rheometer.

For the Plate-on-Plate measurements, results were obtained for two different distances between the two plates (H) i.e. H = 0.5 [mm] and H = 1.0 [mm] and the measures were retained in torque–angular velocity format to enable direct comparison with CFD simulations. Conversely, Cone-on-Plate data were converted into shear stress versus shear rate. The experimental results are shown as black dots in Figures 2 (a) (25 [°C]) and 2 (b) (80 [°C]), together with different analytical regressions of the Herschel–Bulkley model, which will be discussed in the following section. As a first observation, at elevated temperatures and for shear rates below 10^1 [s^{-1}], the Herschel–Bulkley model does not adequately capture the grease behavior.

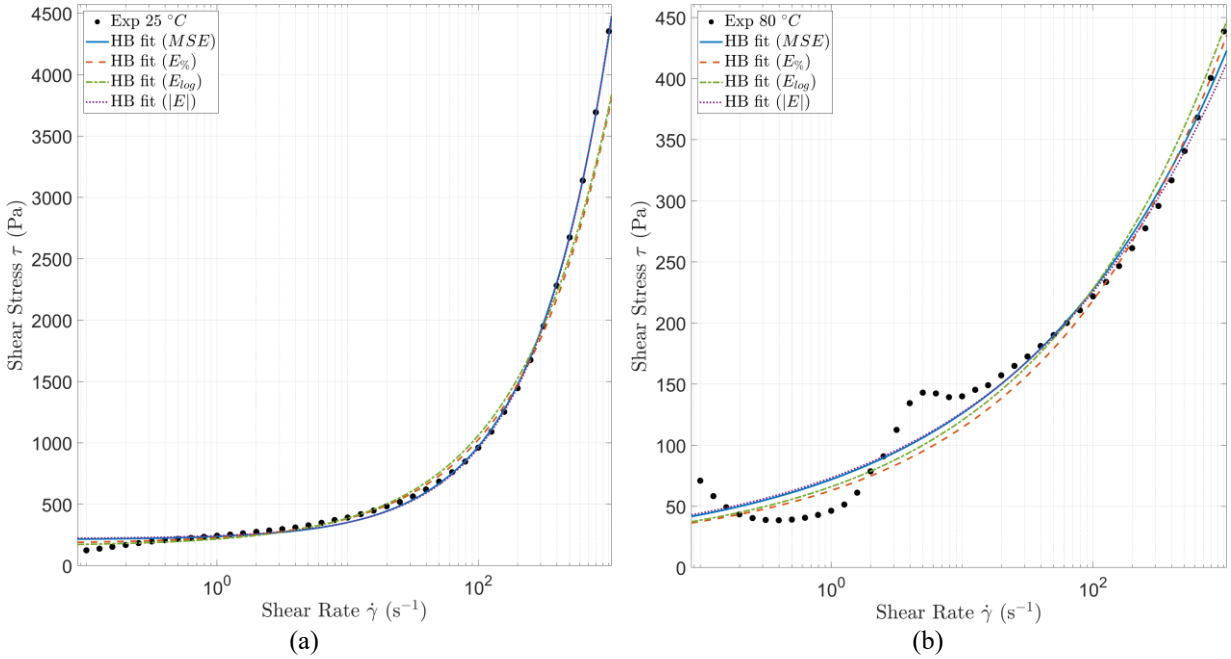

FIGURE 2. Cone-on-Plate: Experimental vs Analytical for different regression methods and temperatures 25°C (a) and 80°C (b).

With respect to regression strategies, four different error minimization approaches were compared. Traditionally, either the mean squared error (MSE, Eq. 3) or the absolute error (Eq. 4) is employed. However, these methods tend

to favor fitting accuracy at high shear rates, often at the expense of correctly representing low shear rate behavior. To overcome this limitation, alternative methods were considered, namely percentage error minimization (Eq. 5) and logarithmic error minimization (Eq. 6), the latter being particularly suitable since the dataset spans several orders of magnitude in shear rate. The results of the regression analyses are summarized in Tables 1 and 2, which also report the corresponding R^2 and Mean Absolute Percentage Error (MAPE) values. Based on these comparisons, the parameters obtained via logarithmic error minimization were selected for further analyses, as this approach provided the best overall trade-off between R^2 and MAPE. Nevertheless, comparable performance was also achieved with the percentage error minimization approach.

$$MSE = \sum[(\tau_0 + K \cdot \dot{\gamma}^n) - \tau]^2 \tag{3}$$

$$|E| = \sum|(\tau_0 + K \cdot \dot{\gamma}^n) - \tau| \tag{4}$$

$$E_{\%} = \sum \left|\frac{(\tau_0 + K \cdot \dot{\gamma}^n) - \tau}{\tau}\right| \tag{5}$$

$$E_{log} = \sum[log(\tau_0 + K \cdot \dot{\gamma}^n) - log(\tau)]^2 \tag{6}$$

TABLE 1. Herschel-Bulkley Parameters at 25°C for Different Regression Method

Method	τ_0 [Pa]	K [Pa·s^n]	n [-]	R^2 [-]	MAPE
MSE	211	25.9	0.73	0.9988	9.69
$\|E\|$	220	23.6	0.75	0.9988	10.3
$E_{\%}$	180	48.9	0.62	0.9787	8.19
E_{log}	160	57.3	0.60	0.9810	8.72

TABLE 2. Herschel-Bulkley Parameters at 80°C for Different Regression Method

Method	τ_0 [Pa]	K [Pa·s^n]	n [-]	R^2 [-]	MAPE
MSE	10.0	61.9	0.27	0.9770	16.9
$\|E\|$	10.2	63.2	0.27	0.9761	17.3
$E_{\%}$	12.8	50.2	0.31	0.9699	15.6
E_{log}	10.7	55.4	0.30	0.9718	15.9

CFD MODELING

The CFD modeling of both the Cone-on-Plate and Plate-on-Plate configurations, at gap heights of H = 0.5 [mm] and H = 1.0 [mm], was performed using the open-source finite volume software OpenFOAM®. In total, six models were developed, combining three geometries with two operating temperatures. Each model was simulated under the angular velocities as those employed in the experimental campaign, providing as outputs not only the torque exerted by the grease on the rotating surface of the rheometer but also the full distribution of pressure, velocity, shear rate, and other relevant fields within the computational domain. Fluid properties were defined according to the calibration data obtained for the two temperatures under investigation. Regarding the viscosity at zero shear rate, this parameter was set to 10,000 [Pa·s] in order to ensure that the Herschel–Bulkley model was effectively applied across the entire domain. With this value, it can be readily verified that for shear rates higher than 10^{-2} [s^{-1}], the Herschel–Bulkley model predicts lower viscosities since the viscosity calculated via the Herschel–Bulkley is always lower then μ_0 in the modeled volume.

To reduce computational effort while preserving accuracy, the domain was modeled as a 2° sector, exploiting the cyclic symmetry of the system. A small central portion was removed to avoid the use of triangular elements, a simplification justified by its negligible influence on the resulting torque. The modeled domain included both the volume beneath the rotating element and an external region, thus accounting for the realistic grease behavior near

the instrument's edge (Fig. 3). This strategy also enabled the use of a two-phase (grease–air) solver, which offers two main advantages: first, it allows validation of a solver that can later be extended to practical cases, e.g. bearings, where grease is often studied in the presence of air; second, it improves the accuracy of flow predictions near the rheometer boundaries.

All computational grids were composed exclusively of hexahedral cells. Mesh quality was ensured by checking an aspect ratio below 6, a maximum skewness lower than 0.65, and a maximum non-orthogonality below 33. The cell count was determined through mesh sensitivity analyses. In the Cone-on-Plate model, the grid consisted of 5,175 cells, including 10 cells across the grease thickness and three cells in the angular discretization. For the Plate-on-Plate configuration, 29,795 cells were used for H = 0.5 [mm] and 65,180 cells for H =1.0 [mm], with angular discretization of five cells in both cases. The grease layer was modeled with consistent element sizes, resulting in 15 cells for the smaller gap and 30 cells for the larger one.

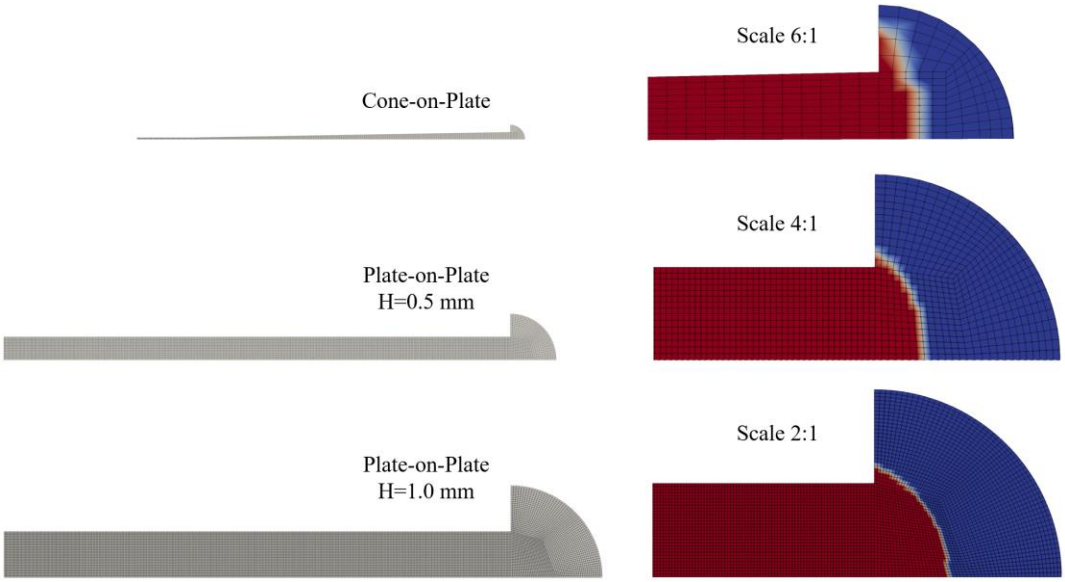

FIGURE 3. Mesh and Initial Conditions (red = grease, blue = air) of the Computational Domain

Boundary conditions included cyclic symmetry on the lateral sides, a prescribed rotational velocity on the moving surfaces, and a no-slip condition on the stationary plates (Fig. 4). At the outer boundary, atmospheric pressure was imposed, allowing for fluids inlet and outlet. The initial phase distribution was set according to the experimental observations. The torque acting on the upper cylindrical surface was not included in the post-processing.

The two-phase solver was defined as incompressible, due to the low velocities and forces involved, and laminar, as the high viscosity of the grease dominated over inertial effects. The system was treated as isothermal, with temperature controlled externally by the rheometer, and transient, to enable application to future simulations of bearing geometries. Although a steady-state solver could have been employed, it was deemed less useful for subsequent studies. The governing equations—continuity, momentum conservation, and volume fraction transport—were solved within this framework.

Simulations were conducted under the same operating conditions as in the experimental campaign. A variable time step was adopted, with the Courant number limited to 0.5 to ensure both high computational efficiency and numerical stability. Convergence was considered achieved either after 10 seconds of simulated physical time, corresponding to the duration of the experimental measurements, or when the torque variation over fifty consecutive time steps fell below 0.1%.

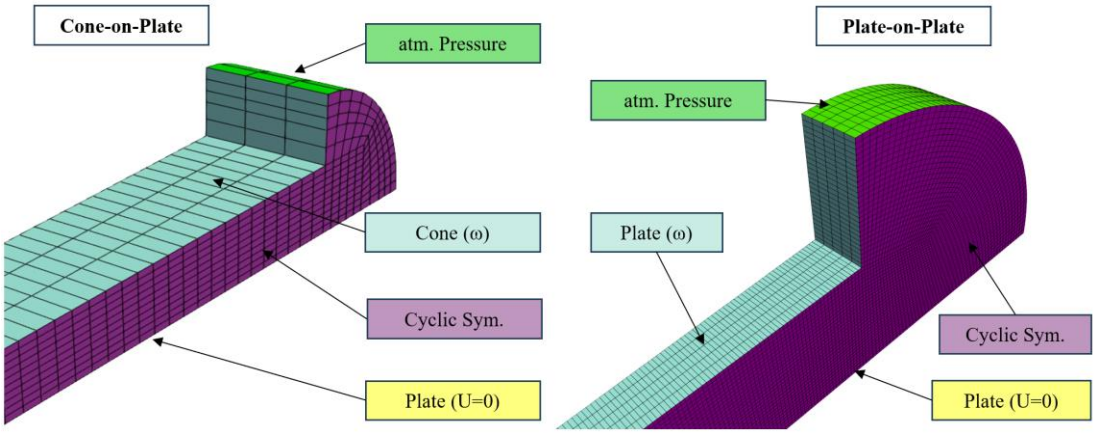

FIGURE 4. Boundary Conditions for Different Configurations

RESULTS AND DISCUSSIONS

Cone-on-Plate Results

In this section, the results of the Cone-on-Plate model are presented to assess its consistency. Two validation checks were performed: the first concerned the shear rate within the fluid volume beneath the cone, and the second compared the torque predicted by CFD with both analytical and experimental values. With regard to the first check, the simulations showed that the variation of shear rate within the region of interest remained below 1% with respect to the theoretical value. Minor deviations were observed near the central area (close to the rotational axis), where the cone approaches a flat geometry, and at the outer edge due to boundary effects; however, these had only a negligible influence on the overall torque. This indicates that the model is highly consistent with the calibration conditions.

Such consistency is further supported by the second check, shown in Fig. 5, where the CFD torque results (red square markers) align almost perfectly with the analytical predictions of the Herschel–Bulkley equations (blue line). This confirms that the closer the analytical model matches the experimental data, the lower the errors expected in the CFD calculations.

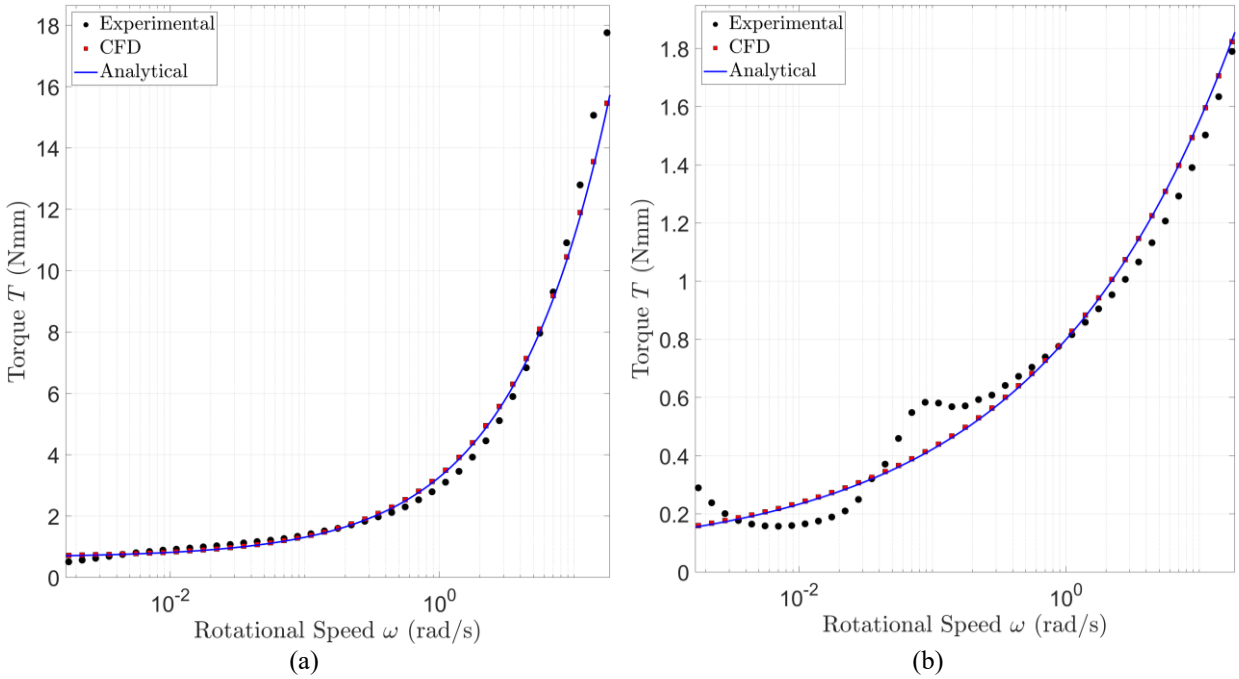

FIGURE 5. Experimental vs Analytical vs CFD results for 25°C (a) and 80°C (b) for Cone-on-Plate

Plate-on-Plate Results

In this section, the results obtained for the Plate-on-Plate configuration are presented. Figure 6 illustrates, as an example, the shear rate distribution within the investigated domain for the same rotational speed (ω=53.93 $[rad/s]$) and temperature (25 [°C]), but with two different gap heights: H = 0.5 [mm] and H = 1.0 [mm]. The figure clearly shows that the shear rate varies linearly with both radius and height. Indeed, when using a vertical scale corresponding to half the gap thickness (H = 0.5 [mm]), the results are very similar to those obtained with H = 1.0 [mm]. An edge effect near the outer boundary is also evident in both cases.

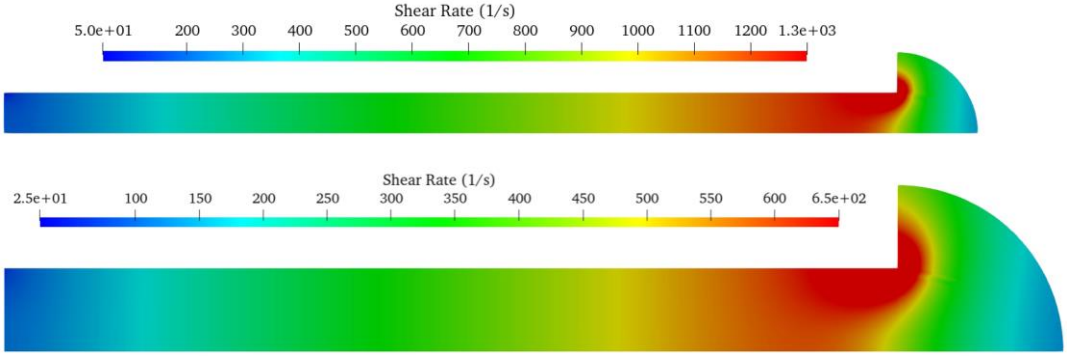

FIGURE 6. Example of shear rate field at ω=53.93$[rad/s]$ and temperature of 25 [°C] in Plate-on-Plate configuration H = 0.5 [mm] (upper), H = 1.0 [mm] (lower)

Figures 7 and 8 compare the CFD predictions with experimental results in terms of rotational speed versus torque. Figure 7 reports the results for H = 0.5 [mm], while Figure 8 refers to H = 1.0 [mm]. In both cases, the results are presented at two different temperatures: 25 [°C] (a) and 80 [°C] (b).

For H = 0.5 [mm] at 25 [°C] (Fig. 7 (a)), the agreement between CFD and experiments is very good. The curves show similar trends, and the numerical values differ by less than 8% for rotational speeds above 25 [rad/s]. The mean percentage error is 6%, with a maximum error of 16% at the lowest speed. In general, CFD tends to overestimate torque at higher angular velocities. At 80 [°C] (Fig. 7 (b)), the agreement remains satisfactory, with a mean error of 3.3% and a maximum error of 14% at the lowest speed, although the CFD and experimental trends deviate slightly.

For the larger gap (H = 1.0 [mm]), similar considerations apply. At 80 [°C] (Fig. 8 (b)), the mean error is 4.6%, with a maximum error of 10.9% at the lowest speed, again with CFD generally overestimating torque. However, at 25 [°C] (Fig. 8a), the CFD results deviate more significantly from the experiments. In this case, the CFD torque increases more rapidly than the experimental measurements, leading to larger discrepancies at higher rotational speeds. The mean error is 15.8%, with a maximum error of 18.5% at the highest speed.

This discrepancy prompted the authors to perform additional numerical tests. Specifically, CFD simulations were carried out using a sector model without the upper dome present in the original geometry, in order to minimize edge effects. These tests produced slightly improved results, but the mean error was reduced by no more than 3%, remaining around 12%. Furthermore, alternative Herschel–Bulkley models obtained through different regression strategies were also implemented. As expected, since the current regression strategy already underestimated torque at high rotational speeds compared to the others, these additional models produced even larger errors. The larger gap thickness may introduce temperature gradients, uncontrolled shearing effects, or a non-uniform distribution of the base oil. These hypotheses will need to be verified in future studies.

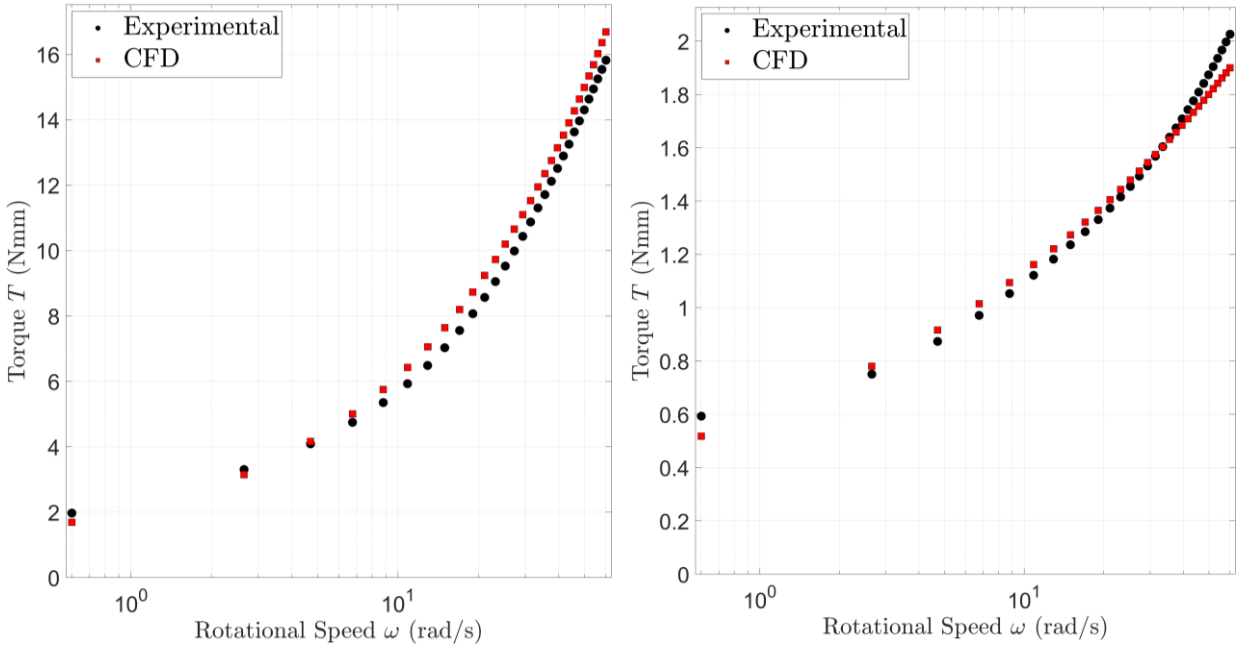

FIGURE 7. Experimental vs CFD results for 25°C (a) and 80°C (b) for Plate-on-Plate, H=0.5 mm

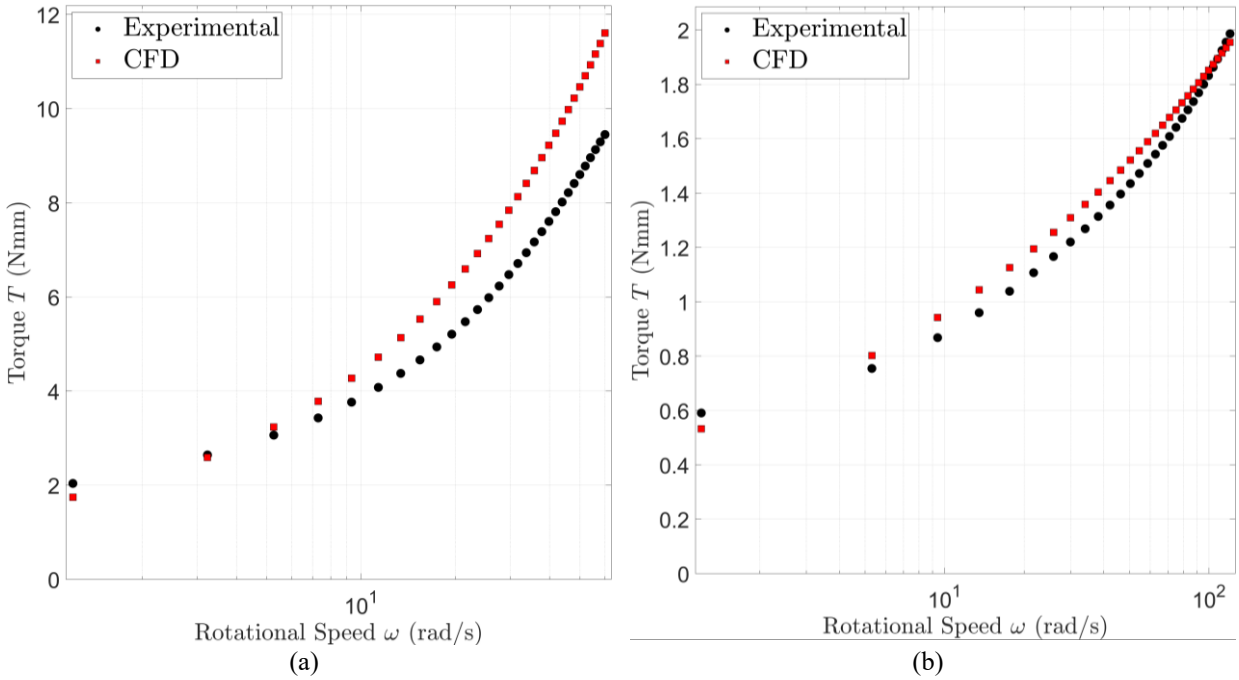

FIGURE 8. Experimental vs CFD results for 25°C (a) and 80°C (b) for Plate-on-Plate, H=1.0 mm

CONCLUSIONS

This study developed and applied a systematic methodology to calibrate the Herschel–Bulkley model for lubricating greases and to verify its implementation in CFD simulations. The results demonstrated that the choice of regression strategy plays a crucial role in determining the model parameters: among the different approaches tested,

logarithmic error minimization provided the best overall balance across the explored shear rate range, while percentage-error-based regression also produced comparable results. Verification with the Cone-on-Plate configuration confirmed the internal consistency of the methodology, as CFD predictions closely matched the analytical Herschel–Bulkley formulation. The Plate-on-Plate configuration, on the other hand, introduced additional complexities due to shear rate gradients and edge effects. At elevated temperature and smaller gap thickness, the agreement between CFD and experiments was very good, with mean errors below 5%. However, at ambient temperature and larger gaps, significant discrepancies emerged, with CFD generally overestimating torque and mean errors exceeding 15%. These differences may be related to the presence of temperature gradients, uncontrolled shearing effects, or a non-uniform distribution of the base oil, hypotheses that will need to be examined in future studies.

The numerical analyses also showed that simplified CFD domains, in which the upper dome was removed, slightly reduced the discrepancies but were not sufficient to fully eliminate them, suggesting that boundary effects linked to geometry remain significant. Another important aspect concerns the choice of the zero-shear viscosity μ_0. In this study, the value selected did not strongly influence the results because the investigated volume was characterized by relatively high shear rates. Nonetheless, a robust methodology for defining μ_0 is required, as this parameter is fundamental for describing grease motion at very low shear rates, which are particularly relevant for reservoir effects in practical applications.

In conclusion, the proposed framework provides a reproducible link between rheometry and CFD through temperature-calibrated Herschel–Bulkley models. While the approach demonstrated promising predictive capability, especially at high shear rates and elevated temperatures, further refinements and modifications are needed to address pre-shear history, extended temperature dependence, aging effects, and low-shear rheology. Addressing these aspects will be essential to enable more reliable, service-oriented simulations of grease-lubricated rolling bearings.

ACKNOWLEDGEMENT

This work was developed within the framework of the HyperCUBE project, financed by Schaeffler Technologies AG & Co. KG, PI F. Concli and the SaveLUBE project, funded by the FSE+ program, ESF2_f3_0006 CUP: B56FF24000090001.

REFERENCES

1. F. Sadeghi, U. Arya, S. Aamer, and A. Meinel, “A review of computational fluid dynamics approaches used to investigate lubrication of rolling element bearings,” *J. Tribol.*, 2024, vol. 146, no. 10, pp. 100801. https://doi.org/10.1115/1.4065663
2. A. Chronis, A. Dubor, E. Cabay, M. S. Roudsari, “Integration of CFD in computational design,” Proceedings of eCAADe 2017, pp. 601-610.
3. L. Maccioni, V. G. Chernoray, F. Concli. “Investigating lubricant behavior in a partially flooded tapered roller bearing: Validation of a multiphase CFD solver for aerated oil sump via particle image velocimetry studies and high-speed camera acquisitions,” *Tribology International*, 2025, vol. 201, pp. 110274. https://doi.org/10.1016/j.triboint.2024.110274
4. S. Aamer, F. Sadeghi, T. Russell, W. Peterson, A. Meinel, and H. Grillenberger, “Lubrication, flow visualization, and multiphase CFD modeling of ball bearing cage,” *Tribol. Trans.*, 2022, vol. 65, no. 6, pp. 1088–1098. https://doi.org/10.1080/10402004.2022.2123420
5. L. Maccioni, L. Rüth, O. Koch, and F. Concli, “Load-independent power losses of fully flooded lubricated tapered roller bearings: Numerical and experimental investigation of the effect of operating temperature and housing wall distances,” *Tribol. Trans.*, 2023, vol. 66, no. 6, pp. 1078–1094. https://doi.org/10.1080/10402004.2023.2254957
6. A. Gonda, D. Großberndt, B. Sauer, and H. Schwarze, “Experimental and numerical investigations of hydraulic losses in rolling bearings under practice-oriented conditions,” *Tribol. Schmier.*, 2018, vol. 65, pp. 7–13.
7. H. Kamat, C. R. Kini, S. B. Shenoy. “Effect of cavitation and temperature on fluid film bearing using CFD and FSI technique: A review”. *Archives of Computational Methods in Engineering*, 2023, vol. 30, no. 3, pp. 1623-1636. https://doi.org/10.1007/s11831-022-09847-z
8. P. M. Lugt. “A review on grease lubrication in rolling bearings”. *Tribol. Trans.*, 2009, vol. 52, no. 4, pp. 470-480. https://doi.org/10.1080/10402000802687940

9. P. M. Lugt, “Modern advancements in lubricating grease technology,” *Tribol. Int.*, 2016, vol. 97, pp. 467–477. https://doi.org/10.1016/j.triboint.2016.01.045
10. S. Zhang, G. Jacobs, S. Vafaei, S. von Goeldel, and F. König, “CFD investigation of starvation behaviors in a grease lubricated EHL rolling contact,” *Forsch. Im Ingenieurwesen*, 2023, vol. 87, no. 1, pp. 353–362. https://doi.org/10.1007/s10010-023-00633-2
11. S. Zhang, G. Jacobs, S. von Goeldel, S. Vafaei, and F. König, “Prediction of film thickness in starved EHL point contacts using two-phase flow CFD model,” *Tribol. Int.*, 2023, vol. 178, p. 108103. https://doi.org/10.1016/j.triboint.2022.108103
12. S. Zhang, B. Klinghart, G. Jacobs, S. von Goeldel, and F. König, “Prediction of bleeding behavior and film thickness evolution in grease lubricated rolling contacts,” *Tribol. Int.*, 2024, vol. 193, p. 109369. https://doi.org/10.1016/j.triboint.2024.109369
13. D. Fischer, S. von Goeldel, G. Jacobs, and A. Stratmann, “Numerical investigation of effects on replenishment in rolling point contacts using CFD simulations,” *Tribol. Int.*, 2021, vol. 157, p. 106858. https://doi.org/10.1016/j.triboint.2021.106858
14. J. Wang, M. P. Pandya, and F. Greco, “Detection of active grease reservoirs in bearings by CFD,” *Tribol. Int.*, 2023, vol. 179, p. 108146. https://doi.org/10.1016/j.triboint.2022.108146
15. P. M. Lugt and S. Velickov, J. H. Tripp. “On the chaotic behavior of grease lubrication in rolling bearings”. *Tribol. Trans.*, 2009, vol. 52, no. 5, pp. 581-590. https://doi.org/10.1080/10402000902825713
16. K.R. Sathwik Chatra and P. M. Lugt. The process of churning in a grease lubricated rolling bearing: Channeling and clearing. *Tribol. Int.*, 2021, vol. 153, pp. 106661. https://doi.org/10.1016/j.triboint.2020.106661
17. K. S. Chatra, J. A. Osara, P. M. Lugt. Impact of grease churning on grease leakage, oil bleeding and grease rheology. *Tribol. Int.*, 2022, vol. 176, pp. 107926. https://doi.org/10.1016/j.triboint.2022.107926
18. K. S. Chatra, J. A. Osara, P. M. Lugt. The lubrication mechanism behind the transition from churning to bleeding in grease lubricated bearings–Experimental characterization. *Tribol. Int.*, 2023, vol. 183, pp. 108375. https://doi.org/10.1016/j.triboint.2023.108375
19. ISO 2137:2007, Petroleum products — Lubricating greases and petrolatum — Determination of cone penetration, ISO, Geneva.
20. ASTM D217-21, Standard Test Methods for Cone Penetration of Lubricating Grease, ASTM International, West Conshohocken, PA.
21. G. M. Gow. “The CEY to grease rheology,” *Trans. Mech. Eng.*, The Institution of Engineers, Australia, Special Issue Tribology, vol. ME16, no. 3, pp. 202–205, 1991.
22. I. Couronné, G. Blettner, and P. Vergne, “Rheological behavior of greases: Part I—Effects of composition and structure,” *Tribol. Trans.*, vol. 43, no. 4, pp. 619–626, 2000. https://doi.org/10.1080/10402000008982386
23. A. W. Sisko, “The flow of lubricating greases,” *Ind. Eng. Chem.*, 1958, vol. 50, pp. 1789–1792. https://doi.org/10.1021/ie50588a042
24. K. D. Bogie and J. Harris, “The rheology of greases,” *Rheol. Acta*, 1968, vol. 7, pp. 255. https://doi.org/10.1007/bf01985786
25. H. E. Mahncke and W. Tabor, “A simple demonstration of flow type greases,” *Lubr. Eng.*, 1955, vol. 11, pp. 22.
26. C. R. Singleterry and E. E. Stane, “Rheological properties of lubricating greases,” *Colloid. Sci.*, 1951, vol. 6, pp. 171. https://doi.org/10.1016/0095-8522(51)90037-2
27. T. C. Papanastasiou. “Flows of materials with yield”. *Journal of rheology*, 1987, vol. 31, no. 5, pp. 385-404. https://doi.org/10.1122/1.549926
28. W. Herschel and R. Bulkley, “Measurement of consistency as applied to rubber-benzene solutions,” *Am. Soc. Test. Mater.*, Proc., 1926, vol. 26, pp. 621–633.
29. M. N. Mastrone and F. Concli, “CFD simulation of grease lubrication: Analysis of the power losses and lubricant flows inside a back-to-back test rig gearbox,” *J. Non-Newtonian Fluid Mech.*, 2021, vol. 297, pp. 104652. https://doi.org/10.1016/j.jnnfm.2021.104652
30. A. Raj, C. Sarkar, and M. Pathak, “Thermal and multiphase flow simulations of polytetrafluoroethylene-based grease flow in restricted geometry,” Proc. Inst. Mech. Eng. *J: Eng. Tribol.*, 2022, vol. 236, no. 1, pp. 80–89. https://doi.org/10.1177/13506501211009406
31. T. Noda, K. Shibasaki, Q. J. Wang. “X-ray ct imaging of grease behavior in ball bearing and multi-scale grease flows simulation.” In Proceedings of the Society of Tribologists and Lubrication Engineers Annual Meeting and Exhibition, pp. 361-362.

32. T. Noda, K. Shibasaki, S. Miyata, and M. Taniguchi, “X-ray CT imaging of grease behavior in ball bearing and numerical validation of multi-phase flows simulation,” *Tribol. Online*, 2020, vol. 15, no. 1, pp. 36–44. https://doi.org/10.2474/trol.15.36
33. B. Wang, Z. Wang, C. Sun, and Y. Wu, “Numerical investigation of the heat-fluid characteristic inside high-speed angular contact ball bearing lubricated with grease,” *Int. J. Eng.*, 2021, vol. 34, no. 5, pp. 1313–1320. https://doi.org/10.5829/ije.2021.34.05b.26
34. C. Fu, T. Chen, H. Yang, H. Li, Y. Li, Y. Zhang, W. He, H. Cong. “Analysis of Temperature Characteristics of Double-Row Spherical Roller Bearings Based on CFD.” Lubricants, 2025, vol. 13, no. 2, pp. 85. https://doi.org/10.3390/lubricants13020085